Diffraction from two-dimensional vicinal surfaces with noncolliding meandering steps

Joachim Wollschläger and Mats Larsson*
Institut für Festkörperphysik, Universität Hannover Appelstrasse 2, D-30167 Hannover, Germany
(Received 7 March 1997; revised manuscript received 16 October 1997)

We present a diffraction pattern analysis for vicinal surfaces with meandering noncolliding steps, so that the fluctuations of adjacent steps are not correlated. For these conditions, we evaluate the shape of the diffuse scattering (additional to sharp peaks due to the long-range order of the steps), and show that the root-mean-square width, the kink density, and the correlation of the individual meandering steps can be obtained from the diffuse scattering for different scattering conditions due to the intrastep correlation. The surface morphology is generated by Monte Carlo simulations performed at various temperatures until the kink density is equilibrated but the steps do not collide. This enables us to compare the direct statistical analysis of the surfaces with the diffraction analysis. We demonstrate that the agreement is excellent. Furthermore, we discuss how these results can be applied to the analysis of diffuse x-ray diffraction from multilayers with noncorrelated interfaces. [S0163-1829(98)06020-2]

I. INTRODUCTION

The roughness of surfaces has been studied very intensively during the last years, since it plays a dominant role in many physical and chemical processes at surfaces. Microscopic and diffraction techniques have been applied to study the surface roughness at equilibrium and far from it (e.g., surfaces of epitaxial films). While microscopic techniques provide information about roughness details, one obtains mainly statistical averages and correlations from diffraction experiments. Thus both techniques are complementary, and it is very useful to combine both. Using the insight obtained from microscopic pictures simplifies the analysis of diffraction pattern and spot profiles.

Since diffraction techniques do not directly provide an image of the surface morphology, one has to model surfaces with defects, and study their impact on the diffraction pattern. Evaluating diffraction spots from these surfaces and analyzing their shape, one is able to interpret experimental diffraction patterns with respect to surface defects as atomic steps. The spot profile analysis for one-dimensional (1D) stepped surfaces is well developed. It has been demonstrated that the spot profiles depend on both the scattering condition and the correlation of surface atoms.[1] Assuming that the sizes of adjacent terraces are not correlated, it has been shown that the spot profile depends only on the terrace size distribution at the out-of-phase condition where adjacent terraces interfere destructively.[1–3] While the spot profiles are broad for wide terrace size distributions, they show a splitting into more or less broad satellites for sharp distributions.[1,4–6]

These evaluation techniques are not well suited to study two-dimensional correlation effects of ''real'' surfaces. In the meantime, however, Monte Carlo (MC) simulations provide not only more insight into studying processes such as diffusion, nucleation of islands, etc. on surfaces, but they are also a very efficient tool to study the effect of the surface morphology on diffraction spots. For instance, they are applied to investigate growth on nonvicinal surfaces in both the submonolayer and multilayer regime.[7–10]

While these investigations are focused mainly on the influence of diffusion barriers on the growth morphology, vicinal surfaces are well suited to study the meandering of steps at thermal equilibrium involving, e.g., the energy to create kinks and the interaction between adjacent steps. But not only from this point of view but also for diffraction spot analysis, vicinal surfaces are much simpler than rough low-index surfaces where the topography is dominated by islands forming closed loops of atomic steps. Thus both the island diameter and the island distance distribution influence the diffraction spots. On the other hand, for vicinal surfaces, the steps have a preferential direction, so that the rough surface can be described by the meandering of steps, and only the intracorrelation of the position of the same step and the intercorrelation of the position of nonidentical steps enter into the spot evaluation. Beside analytic models,[11–14] which are based on different interactions of step atoms within one step and between different steps, MC simulations[15–17] have also been used to study the influence of step meandering on the diffraction pattern.

Basing on the terrace-ledge-kink model and considering only the anisotropic interaction between nearest-neighbor step atoms of the same step and of next-neighbor steps, Villain, Grempel and Lapujoulade distinguished two different phases for the morphology of vicinal surfaces.[11] The phases are characterized by the displacement correlation defined by $g_n(x)=\langle\langle[u_{n+m}(x+x')-u_m(x')]^2\rangle\rangle_{m,x'}$ for large distances. Here $u_n(x)$ is the displacement of the nth step running in the x direction, while the brackets denote averaging with respect to m and x' (for more details, also see Sec. II). For the low-temperature phase the steps are not straight, but the fluctuations are finite, so that one obtains the limit $g_0(x)=\langle[u_m(x+x')-u_m(x')]^2\rangle_{x'}\to 2w^2$ for $x\to\infty$ [w denotes the root-mean-square (rms) width of the step]. This saturation effect cannot be observed for the high-temperature phase where the displacement correlation diverges logarithmically. This behavior has been corroborated by MC simulations.[15]

Since the step fluctuations are finite for the low-temperature phase and diverge for the high-temperature

phase, the inverse rms width w can be used as order parameter for this (Kosterlitz-Thouless) phase transition. This motivates our nomenclature as a correlation with long-range order for the low-temperature phase, and a correlation with short-range order for the high-temperature phase (an analog to the nomenclature of two-dimensional phase transitions).

The diffraction spot profiles for both phases are significantly different. Above the critical temperature the logarithmic divergence is reflected by power-law profiles with temperature-dependent exponents. Below the critical temperature the profiles split into two components: a sharp peak due to the long-range order and a diffuse scattering due to the step roughness. Up to now, however, the diffuse scattering for the low-temperature vicinal surface with long-range order has not been analyzed in detail, while the temperature-dependent exponent of the power-law profiles for the high-temperature phase has also been studied experimentally to determine the critical temperature of the roughening transition T_R.[18–21] It has also been reported that the roughening can be obtained from the vanishing of the sharp central peak of the low temperature phase at T_R.[22,23]

Bartelt, Einstein, and Williams reported that the logarithmic diverging displacement correlation can only be observed for distances larger than the average collision distance between adjacent steps.[14] For shorter distances it increases linearly. Consequently, the spot profiles show only a power-law behavior for small scattering vectors, while the profiles have a Lorentzian profile for large scattering vectors.

The goal of this paper is to analyze the spot profiles from vicinal surfaces in the low-temperature phase ($T<T_R$), where the steps do not collide and the rms width of the fluctuating steps are small compared to the average step-step distance. For that purpose we compare analytic closed-form spot profiles with spot profiles obtained from MC simulations. In a previous paper, we demonstrated that the attenuation of the sharp peak of the spot profiles can be used to analyze the rms width of noncolliding steps.[24] The main result of our studies is that, starting the MC simulation with straight equidistant steps, the kink density saturates after some time although the steps do not collide. Therefore we attribute the investigated phase to the low-temperature phase with long-range order below the roughening temperature. The temporal evolution of the rms width shows a power-law behavior with different exponents before and after the kink density has saturated.

In this paper we emphasize the analysis of the diffuse shoulder. We demonstrate that one can obtain detailed information about the statistics of the fluctuating steps. The half-width of the spot profiles perpendicular to the steps are governed by the rms width of the fluctuating steps. The half-widths of spot profiles recorded parallel to the parallel steps, however, depend on the scattering condition. The half-widths of the the spot profiles recorded at the center of the Brillouin zone are determined by the correlation length ξ. They are sensitive to the kink density for spot profiles at the boundary of the Brillouin zone.

The paper is organized as follows. In Sec. II, we initiate the evaluation of the diffraction pattern for vicinal surfaces followed by the analysis of the diffuse scattering with respect to the rms width, the correlation length, and the kink density of the meandering steps (Sec. III). After a short description of the applied Monte Carlo model (Sec. IV), we demonstrate in Sec. V that the assumption of noncorrelated step fluctuations is in excellent agreement with the calculated step roughness.

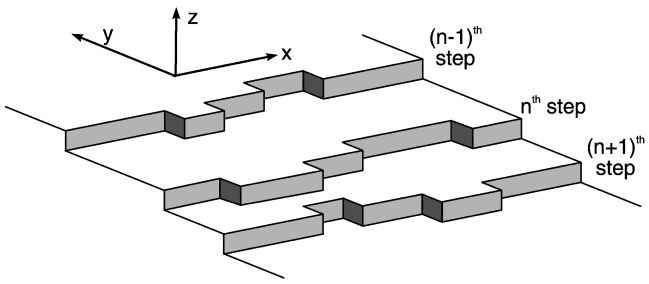

FIG. 1. Schematic drawing of a vicinal surface with meandering steps.

II. EVALUATION OF THE DIFFRACTION PATTERN FOR VICINAL SURFACES

For the sake of simplicity, we base the evaluation of the diffraction pattern on the simple cubic (sc) lattice. This implies that the higher-order spots have the same phase dependence as the specular (00) spot has. Most of the reported experiments have been carried out at surfaces of face-centered-cubic (fcc) and body-centered-cubic (bcc) crystals. If, however, one confines the diffraction spot analysis to the first Brillouin zone, *all* lattices show an identical behavior. The effect on higher Brillouin zones will be discussed later.

We suppose that the step train of the vicinal surface runs into the y direction with ascending step height, implying that the steps are parallel to the x direction (cf. Fig. 1). Within the kinematic approximation the amplitude of the wave scattered at this surface is

$$A(K_z,K_y,K_x)=\sum_n e^{iK_z dn}\sum_x e^{iK_x ax}\frac{e^{iK_y R_{n+1}(x)}-e^{iK_y R_n(x)}}{1-e^{iK_y a}}, \tag{1}$$

where $R_n(x)$ and $R_{n+1}(x)$ denote the position of the nth and $(n+1)$th meandering steps, respectively, confining the nth terrace. Here x is an integer, so that ax is the position of the step atom parallel to the step. The scattering vector has been split into the scattering vector perpendicular to the terraces (z direction) of the vicinal surface K_z, the lateral scattering vector K_y perpendicular to the steps (y direction, the direction of the step train), and the lateral scattering vector K_x parallel to the steps (x direction). Equation (1) supposes that the step position is a single-value function neglecting overhangs. Additional islands on top of the vicinal terraces are also excluded.

For the scattering experiment, however, not the scattering amplitude but the lattice factor

$$\begin{aligned}G(K_z,K_y,K_x)&=|A(K_z,K_y,K_x)|^2\\&=\frac{1-\cos(K_z d)}{1-\cos(K_y a)}\sum_n e^{iK_z dn}\sum_x e^{iK_x ax}\\&\quad\times\langle\langle e^{iK_y[R_{n+m}(x+x')-R_m(x')]}\rangle\rangle_{m,x'}\end{aligned} \tag{2}$$

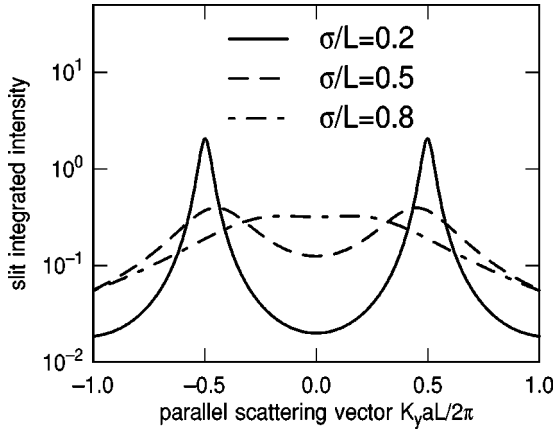

FIG. 2. Diffraction pattern for a 1D surface with noncorrelated sizes of adjacent terraces. Due to the short-range order the peaks do not show sharp profiles. Conversely, the half-width of the peaks increase with increasing width of the terrace size distribution (increasing σ).

is important where $\langle\langle \cdots \rangle\rangle$ denotes averaging with respect to the step index m and the lateral position in the direction of the step x'.

A. One-dimensional vicinal surfaces: step correlation effects

Above we discussed the difference between long- and short-range order. Thus, here, we want to show the impact of these correlations on the diffraction from quasi-1D surfaces, since the spot profile analysis by the analytic closed-form profile evaluation works very well for these ''artificial'' surfaces. We emphasize that these models are well suited to obtain a better insight into the *diffraction* effects but not into the *physics* of the roughening.

Especially vicinal surfaces with short-range order (the step position is determined from the position of the adjacent terraces via the terrace size distribution) have been studied intensively.[1,4,6] The analysis is based on the 1D form of the lattice factor shown in Eq. (2), neglecting the dependence on x and x'. The main result of these studies is that the diffraction spots broaden and shift to the center of the Brillouin zone, as shown in Fig. 2 for the out-of-phase condition. Generally, both the broadening and the shift depend on the scattering condition. The short-range order implies that the correlation vanishes gradually with increasing distance between the two steps. Therefore, this model is equivalent to a nonconfined random walk.

Here we study a different model for surfaces with long-range order. Due to the long-range order the uncertainty of the step position cannot increase infinitely. Comparing the distance between two steps $R_{n+m}-R_m$, one expects that the position is not too different from the distance naL, where L denotes the *number* of atoms between two adjacent steps for an ideally stepped regular vicinal surface. Therefore, it is useful to split the position of the nth step R_n into the position for the regular vicinal surface naL and the displacement u_n with respect to the regular position. For this vicinal surface with long-range order we expect the constant displacement correlation $\langle[u_{n+m}-u_m]^2\rangle=2w^2=2\langle u_m^2\rangle$, except for $n=0$, where the correlation equals zero. Thus the long-range order

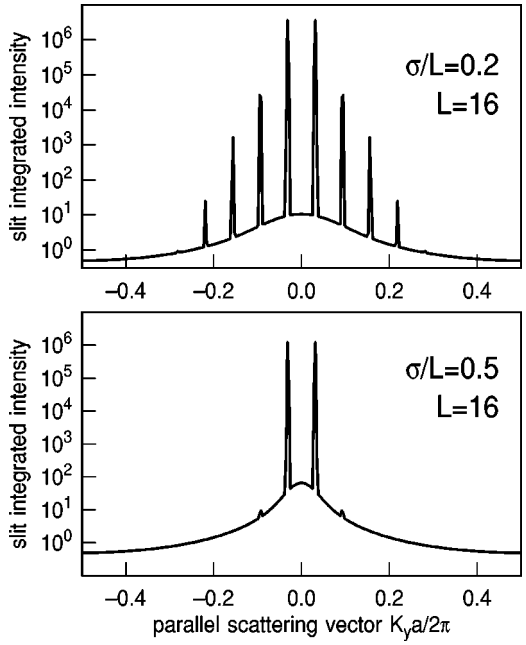

FIG. 3. Diffraction pattern for a 1D surface with long-range order, preserving the position and the half-width of the sharp peaks. The increasing fluctuation of the steps yields an increasing diffuse background and the attenuation of the intensity of the sharp peaks, especially for the higher-order peaks.

model is equivalent to a confined random walk. Of course this model is only useful in the limit $w \ll aL$.

On the other hand, for surfaces with short-range order the displacement correlation diverges via $\langle[u_{n+m}-u_m]^2\rangle \propto n$, at least for small distances, while for larger distances the divergence may be less drastic (cf. the logarithmic divergence expected for the roughening transition).

For the 1D vicinal surface with long-range order (LRO), we obtain

$$G_{LRO}^{1D}(K_z,K_y)=|\beta(K_y)|^2 G_{reg}^{1D}(K_z,K_y) + \frac{1-\cos(K_z d)}{1-\cos(K_y a)}[1-|\beta(K_y)|^2] \quad (3)$$

from Eq. (2), assuming that the displacement of adjacent terraces are not correlated. Here

$$G_{reg}^{1D}(K_z,K_y)=\frac{1-\cos(K_z d)}{1-\cos(K_y a)}\sum_p \delta(K_y aL+K_z d-2\pi p) \quad (4)$$

denotes the lattice factor of a regularly stepped vicinal surface where $\beta(K_y)=\langle e^{iK_y a u_n(x)}\rangle_{n,x}=\Sigma_u p_u e^{iK_y a u}$ denotes the characteristic function (Fourier transform) of the fluctuation distribution p_u. Figure 3 presents typical diffraction pattern for the out-of-phase condition. The sharp equal distant peaks which are expected for regularly stepped surfaces are striking. The intensity of these peaks, however, is attenuated due to the fluctuating step position via the prefactor $|\beta(K_y)|^2$, so that for $\sigma/L=0.5$ the second-order peaks are hardly visible. On the other hand, the intensity of the diffuse shoulder increases, and its shape narrows with increasing rms width w (defined by $w^2=\langle u^2\rangle$). We would like to mention that only the first case $\sigma/L=0.2$ presented in Fig. 3 is reasonable,

because the probability to form overhangs by the noncorrelated step position fluctuations is unlikely. Since this is not the case for $\sigma/L=0.5$, the model and the diffraction pattern are unphysical.

This effect of noncorrelated step fluctuations is very similar to the well-known Debye-Waller effect causing an attenuation of the peaks due to thermally activated atomic vibrations (except for the homogeneously distributed diffuse scattering). Thus the attenuation effect may be called the static Debye-Waller effect, as proposed for the x-ray diffraction from multilayers.[25]

In our previous MC study of the temporal development of the rms width, we have shown that the intensity is attenuated generally by $|\beta(K_y)|^2 \simeq e^{-w^2K_y^2}$ for the sharp central peak close to the center of the Brillouin zone.[24] Here we assume that the fluctuations are Poisson distributed ($p_u = [(w/a)^{2(u+w)}/\Gamma(u+w+1)]e^{-(w/a)^2}$ and $u \geqslant -w$ where $\Gamma(x)$ denotes the γ function). Thus one obtains the attenuation factor

$$|\beta(K_y)|^2 = \exp\left[-2\frac{w^2}{a^2}[1-\cos(K_y a)]\right] \tag{5}$$

to evaluate the diffraction pattern in Fig. 3. Equation (5) matches and confirms the Gaussian behavior for scattering vectors close to the center of the Brillouin zone.

On first sight the diffraction pattern analysis for 1D surfaces seems to be quite academic, since ''real'' surfaces are 2D. However, a simple way to extract the correlation effects presented here for 1D surfaces is to integrate the 2D diffraction pattern in the step direction

$$\begin{aligned} G_{slit}(K_z,K_y) &= \int dK_x G(K_z,K_y,K_x) \\ &= \frac{1-\cos(K_z d)}{1-\cos(K_y a)} \sum_n e^{iK_z dn} \\ &\quad \times \langle\langle e^{iK_y a[R_{n+m}(x')-R_m(x')]}\rangle\rangle_{m,x'}. \end{aligned} \tag{6}$$

In this case only the step positions for a cross section in the step train direction enter the evaluation of the lattice factor [i.e., identical lateral positions x' for both step positions in Eq. (2)], so that the 1D analysis can be applied. Obviously the averaging is with respect to different steps (index m) and cross sections (index x').

B. Two-dimensional surfaces: fluctuation effects

We have established that the 1D vicinal surface with long-range order shows completely different diffraction patterns compared to the diffraction patterns that are known for vicinal surfaces with short-range order. Now we want to extend this analysis to 2D surfaces with long-range order. This means that each individual step may fluctuate individually, and the fluctuations are confined to a region close to the straight nonfluctuating step, so that they do not influence the fluctuations of the adjacent steps.

Equivalent to the 1D case, we split the position $R_n(x)$ of the nth fluctuating step into the average (with respect to x) position $\overline{R_n} = \langle R_n(x)\rangle_x$ and the displacement $u_n(x)$ from the average position. Additionally, we also assume equidistant steps on average ($\overline{R_n} = naL$), so that Eq. (2) can be transformed to

$$\begin{aligned} G(K_z,K_y,K_x) &= \frac{1-\cos(K_z d)}{1-\cos(K_y a)} \sum_n e^{i(K_z d + K_y aL)n} \\ &\quad \times \sum_x e^{iK_x ax} \langle\langle e^{iK_y a[u_{n+m}(x+x')-u_m(x')]}\rangle\rangle_{m,x'}. \end{aligned} \tag{7}$$

Assuming nonmeandering steps [$u_n(x) \equiv 0$], the last part of Eq. (7) is equal to 1. Thus one obtains the lattice factor

$$\begin{aligned} G_{reg}^{2D}(K_z,K_y,K_x) &= \frac{1-\cos(K_z d)}{1-\cos(K_y a)} \sum_l \delta(K_x a - 2\pi l) \\ &\quad \times \sum_p \delta(K_y aL + K_z d - 2\pi p), \end{aligned} \tag{8}$$

with sharp peaks on the y axis running through the center of the Brillouin zone for the regularly stepped 2D vicinal surface with terrace size L. The positions of the peaks are equidistant, but depend on the scattering vector K_z.

Similar to the 1D case, the lattice factor can be split into one part with sharp peaks and one diffuse part:

$$\begin{aligned} G(K_z,K_y,K_x) &= |\beta(K_y)|^2 G_{reg}^{2D}(K_z,K_y,K_x) \\ &\quad + G_{diff}(K_z,K_y,K_x), \end{aligned} \tag{9}$$

assuming that the fluctuations of the individual steps have no impact on neighbor step fluctuations. The attenuation factor $|\beta(K_y)|^2$ of the sharp peaks is defined in the same way as for the 1D surface [cf. Eq. (5)]. Thus one can also transform the results mentioned above to the 2D case.

In the following we will concentrate our study on the diffuse scattering. As mentioned above we assume no correlation of neighbor step fluctuations. However, we will not neglect correlations within the same step (i.e., intrastep correlations) including interaction between kinks and that the bending of the steps is governed by the stiffness of the step. With these assumptions the last term of Eq. (7) $\langle e^{iK_y a[u_{n+m}(x+x')-u_m(x')]}\rangle_{x'}$ vanishes except for $n=0$, and the diffuse scattering

$$G_{diff}(K_z,K_y,K_x) = \frac{1-\cos(K_z d)}{1-\cos(K_y a)} \langle G_m(K_y,K_x)\rangle_m \tag{10}$$

is obtained with

$$G_m(K_y,K_x) = \sum_x e^{iK_x ax} \langle e^{iK_y a[u_m(x+x')-u_m(x')]}\rangle_{x'}.$$

For symmetry reasons, we suppose that the evolution of all steps follows the same statistics, i.e., $G_m(K_y,K_x)$ does not depend on a particular step, and can be replaced by

$$G_{single}(K_y,K_x) = \sum_x e^{iK_x ax} \langle e^{iK_y a[u(x+x')-u(x')]}\rangle_{x'}, \tag{11}$$

with $u(x) \equiv u_m(x)$ for all m, which gives the lattice factor

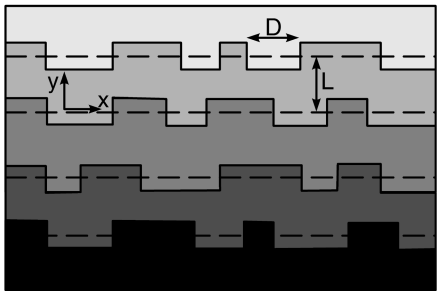

FIG. 4. Schematic model for a vicinal surface with a step meandering within two levels. The dashed lines show the average step position yielding $u=\pm\frac{1}{2}$ and $v=\pm 1$ [cf. Eq. (13)].

$$G_{diff}(K_z,K_y,K_x)=\frac{1-\cos(K_z d)}{1-\cos(K_y a)}G_{single}(K_y,K_x). \tag{12}$$

The mathematical form for $G_{single}(K_y,K_x)$ is equivalent to the one for a 1D surface which is often discussed in literature. Also, the physical interpretation is similar if one substitutes the lateral displacement $u(x)$ by the vertical displacement involved in the spot profile analysis of 1D surfaces. This equivalence is also clear from Fig. 4, showing the top view on a vicinal surface with small displacements: each fluctuating step looks like a 1D (or cross section of a two-dimensional) randomly stepped surface.

Therefore, we would like to apply the well-developed theory for spot profile analysis of 1D surfaces to the spot profile analysis for noncolliding fluctuating steps. Consequently one also has to transform the scattering conditions for the 1D surfaces: The scattering vector $K_\perp$ *vertical* to the surface has to be replaced by the lateral scattering vector K_y *vertical* to the steps and the scattering vector $K_\parallel$ *parallel* to the 1D surface by the lateral scattering vector K_x *parallel* to the steps. Therefore the vertical in-phase condition $K_\perp=2\pi n/d$ transforms to a line scan at $K_y=0$, crossing the center of the Brillouin zone and running parallel to the step directions. The vertical out-of-phase condition $K_\perp=[(2n+1)\pi/d]$ is equivalent to a line scan parallel to the steps at the Brillouin-zone boundary ($K_y=\pm\pi/a$). We will demonstrate that cross sections of the diffuse scattering at these different scattering conditions are sensitive to different morphology parameters, e.g., the kink density or the correlation length.

III. ANALYSIS OF THE DIFFUSE SCATTERING FOR NONCORRELATED FLUCTUATIONS

A. General form

Equation (12) demonstrates that the diffuse scattering is affected by the details of the displacement $u(x)$. Thus the correlation effects between the displacements at different sites are important to determine the exact profile of $G_{single}(K_y,K_x)$. Following the basic spot profile evaluation for 1D randomly stepped surfaces introduced in Ref. 1, one has to consider only correlation effects for constant difference au with integer u, since we assume that all step atoms are on lattice sites. For each difference one has to introduce a *partial* correlation function $\varphi_u(x)$, describing generally the lateral dependence of the displacement fluctuations. These functions are defined by the well-known pair-correlation functions (defined by the probability that two step atoms separated by the lateral distance x have the displacement difference u) $C(x,u)=C_u[1-\varphi_u(x)]$ where C_v depends on the displacement distribution p_u via $C_v=\Sigma_u p_{u+v}p_v$ with integer v. From these fundamental relationships, we obtain the basic description

$$G_{single}(K_y,K_x)=\sum_v C_v[1-\cos(K_y a v)]\Phi_v(K_x) \tag{13}$$

entering the lattice factor of Eq. (12). The functions $\Phi_v(K_x)$ obeying the normalization $\int dK_x\Phi_v(K_x)=1$ are the Fourier transforms of the partial correlation functions $\varphi_u(x)$ introduced above.

Equation (13) shows that the profiles of line scans parallel to the steps (constant K_y) depend in detail on the scattering vector K_y, the displacement distribution, and the details of the partial lateral correlation. The latter dependence can be eliminated for slit profiles integrated parallel to the steps. One obtains

$$G_{slit}(K_z,K_y)=\frac{1-\cos(K_z d)}{1-\cos(K_y a)}[1-|\beta(K_y)|^2], \tag{14}$$

which is identical to the diffuse scattering for the 1D surface with long-range order [cf. Eq. (3)]. The slit-integrated profiles are influenced only by the rms width w.

Although the evaluation of the diffuse scattering depends on many details of the step fluctuation statistics, we can analyze the diffuse shoulder for certain scattering conditions to obtain information about the step roughness. Thus, before presenting the full analysis with respect to kink density, rms width, correlation length and phase dependence of the diffuse shoulder, we start with a simple model of limited step meandering to explain the main effects one expects for the diffuse scattering from surfaces with noncorrelated meandering steps.

B. Small fluctuations: two-level model

The simplest case is step meandering confined to two levels (cf. Fig. 4). Similar to the submonolayer regime for the growth on flat terraces, this case is the smallest deviation from perfectly smooth straight steps. Although we expect larger displacements for ''real'' fluctuating steps, the ''academic'' case, where forward and backward kinks of length a alternate, is worth studying because it gives insight into the principles of the diffraction analysis for the diffuse shoulder.

For the two-level case, Eq. (13) can be simplified very easily, since only displacement differences $v=\pm 1$ are present, so that the shoulders $\Phi_{\pm 1}(K_x)$ are the only contributions to the diffuse scattering. For symmetry reasons, both shoulders must be identical $[\Phi_{\pm 1}(K_x)=\Phi(K_x)]$, and both levels are equally populated ($p_{\pm 1/2}=\frac{1}{2}$). Inserting these into Eqs. (12) and (13), one obtains the diffuse scattering

$$G_{diff}(K_z,K_y,K_x)=\tfrac{1}{2}[1-\cos(K_z d)]\Phi(K_x), \tag{15}$$

indicating the expected vanishing of the diffuse scattering for the vertical in-phase condition ($K_z d=2\pi n$) and the maximum intensity at the vertical out-of-phase condition [$K_z d=(2n+1)\pi$]. Furthermore, the intensity does not depend on

the lateral scattering vector K_y in the step train direction, so that all cross sections parallel to the steps are identical with respect to both the shape and the maximum intensity.

It has been demonstrated for 1D randomly stepped surfaces that the profile of the diffuse scattering can be evaluated from the terrace size distribution.[1] Applying this concept to the fluctuating steps considered here, the terrace size distribution (the distance between two atomic steps) transforms to the kink distance distribution, so we obtain the profile

$$\Phi(K_x)=\frac{1}{1-\cos(K_x a)}\left[\frac{1-\gamma(K_x)}{1+\gamma(K_x)}+\text{c.c.}\right] \tag{16}$$

for the diffuse scattering, where $\gamma(K_x)$ denotes the characteristic function of the kink distance distribution. For instance, supposing that kinks interact repulsively, short distances are suppressed, so that the kink distance distribution shows a maximum close to the average kink distance $\langle D\rangle$. Therefore one expects that the diffuse scattering has maximum intensity at $K_x \simeq 2\pi/\langle D\rangle$. However, if the kinks do not interact, their positions are distributed randomly, leading to a geometric kink distance distribution, and the characteristic function is

$$\gamma(K_x)=\frac{1}{1-i\langle D\rangle K_x}.$$

Inserting the characteristic function into Eq. (16), one obtains the Lorentzian shape

$$G_{diff}(K_z,K_y,K_x)=\frac{4[1-\cos(K_z d)]}{\kappa^2+K_x^2} \tag{17}$$

for the diffuse scattering, where the half-width depends on the linear kink density $\rho=1/\langle D\rangle$ via $\kappa=2\rho$.

C. General kink density analysis

In contrast to the result obtained for the two-level model, generally the half-width of the diffuse scattering depends on the lateral scattering vector K_y perpendicular to the steps, as shown in Sec. III A. Even if one has randomly distributed kinks but step meandering larger than the lattice constant, the diffuse scattering is governed by several shoulders $\Phi_u(K_x)$ [cf. Eq. (15)], with a Lorentzian shape but a different dependence on K_x (cf. the consideration of Sec. III E).

Therefore, at first sight, it is not clear how the kink density can be evaluated from the diffuse scattering. The solution of this problem comes from the formal equivalence between the diffraction from meandering steps and from 1D randomly stepped model surfaces. It is well known for the 1D models that the *shape* of the diffuse shoulder does not depend on the scattering condition for two-level surfaces while the shape shows differences between in-phase and out-of-phase conditions with increasing surface roughness. Section III B showed that equivalence holds strictly for the two-level excitations of the vicinal steps: the shape of the diffuse shoulder does not depend on K_y.

It is also well known, however, that for one special scattering condition—the vertical out-of-phase condition $K_z d=(2n+1)\pi$—the profile depends only on the terrace size distribution, independent of the number of exposed layers (out-of-phase projection).[26] To apply this concept to vicinal surfaces with meandering steps, we have to consider that the vertical out-of-phase condition is equivalent to the lateral out-of-phase condition $K_y^{out}=\pm\pi/a$ at the boundary of the Brillouin zone. The kink distance distribution of the meandering step is equivalent to the terrace size distribution of the randomly stepped 1D surface. Accordingly, we have to analyze line scans for this scattering condition to obtain in a simple way the information about the kink distance distribution. Only for these line scans is the shape of the diffuse shoulder linked directly to the kink distance distribution, independent of the rms width of the meandering steps. Thus we have found an outstanding scattering condition to determine the kink-kink distance distribution, which may offer more insight into the thermodynamical properties of steps.

In Sec. III B we presented the relation between the average kink-kink distance and the spot profile for a geometric kink-kink distance distribution for the two-level model [Eq. (17)] and can now generalize this result to rougher steps for the lateral out-of-phase condition K_y^{out}:

$$G_{diff}(K_z,K_y^{out},K_x)=\frac{4[1-\cos(K_z d)]}{\kappa_{out}^2+K_x^2}. \tag{18}$$

Here κ_{out} denotes the half-width of the diffuse shoulder at the lateral out-of-phase condition. Accordingly the linear kink density ρ can be evaluated from the full width half maximum (FWHM), which is equal to $2\kappa_{out}=4\rho$.

D. Diffuse scattering close to the center of the brillouin zone

We have demonstrated that information about the kink density can be extracted from the diffuse scattering at the lateral out-of-phase condition $K_y a=(2n+1)\pi$. In this section we show that it is also possible to obtain the correlation length ξ by analyzing the diffuse scattering at the lateral in-phase condition $K_y=0$ (line scans parallel to the steps including the center of the Brillouin zone).

Assuming an exponential form of the lateral correlation, the correlation length ξ is defined via the autocovariance function $\langle u(x+x')u(x')\rangle=w^2\alpha(x)$ of the meandering step position $u(x)$ by

$$\alpha(x)=\exp\left(-\frac{|x|}{\xi}\right), \tag{19}$$

where the brackets $\langle\cdots\rangle$ denote averaging with respect to x'. Equation (19) is related to the earlier defined displacement correlation $g_n(x)$ via $g_0(x)=2w^2[1-\alpha(x)]$. It has been reported that the displacement correlation shows the linear behavior $g_0(x)\simeq[b^2(T)/a]x$ for small lateral distances, where $b^2(T)$ denotes the temperature-dependent diffusivity governing the probability to find a kink for a random walk in the step direction.[27] Approximating the exponential of the autocovariance by a linear function, we obtain the diffusivity $b^2(T)=w^2 a/2\xi$ from the correlation parameters.

Substituting $G_{single}(K_y\simeq 0,K_x)$ in Eq. (12) with the second-order Taylor approximation $G_{single}(K_y\simeq 0,K_x)$

$\simeq K_y^2\Omega(K_x)$ [the power spectrum $\Omega(K_x)$ denotes the Fourier transform of the autocovariance], one obtains the diffuse scattering

$$G_{diff}(K_z,K_y=0,K_x)=2[1-\cos(K_z d)]\Omega(K_x), \quad (20)$$

with

$$\Omega(K_x)=\frac{2w^2\kappa_{in}}{\kappa_{in}^2+K_x^2},$$

where κ_{in} is defined via $\kappa_{in}=\xi^{-1}$. Thus the correlation length ξ can be determined from the half-width of the diffuse scattering at the lateral in-phase condition $K_y=0$ while the peak intensity

$$G_{diff}(K_z,K_y=0,K_x=0)=4[1-\cos(K_z d)]w^2\xi \quad (21)$$

is additionally influenced by the rms width w.

E. Diffuse profiles parallel to the steps

Sections III C and III D showed that the profiles at the center and at the boundary of the Brillouin zone are governed by the correlation length and the average kink-kink distance, respectively. For the two-level model both lengths are identical. This is reflected by the constant diffuse profile for this model. In general, however, both lengths are different. Since the correlation length is larger than the average kink-kink distance, we expect broader profiles at the Brillouin-zone boundary than at the center.

To describe the full dependence of the diffuse shoulder, we apply a recently developed model for intermediate rough nonvicinal surfaces ($0.5<w/a<\infty$), where we obtain a simple analytic formula for the phase dependence of the half-width assuming an analytic form of the *vertical* dependence of the pair-correlation function to the intermediate step fluctuations.[28] Transforming this to the case studied here, the half-width of the diffuse profiles parallel to the steps can be approximated by

$$\kappa(K_y)\simeq\frac{2w^2}{\xi a^2}\frac{1-\cos(K_y a)}{1-|\beta(K_y)|^2} \quad (22)$$

with $|\beta(K_y)|^2=\exp[-2(w^2/a^2)[1-\cos(K_y a)]]$.

Thus one obtains the relation $\kappa_{out}\simeq 4(w^2/a^2)\kappa_{in}$ connecting the half-width κ_{in} at the lateral in-phase condition with the half-width κ_{out} at the lateral out-of-phase condition via the rms width w. This implies that the correlation length depends on both the kink density and the rms width via $\xi=2w^2/\rho a^2$. Substituting this result into the expression for the diffusivity, we find the simple relation $b^2(T)=\rho a^3$ underpinning the intuitive interpretation of the diffusivity as the probability to create a kink during a random walk along the step.

Due to the fact that the slit-integrated intensity can be approximated by

$$G_{slit}^{diff}(K_z,K_y)\simeq 2\kappa G_{diff}(K_z,K_y,K_x=0), \quad (23)$$

the peak intensity of the diffuse shoulder at a vanishing parallel scattering vector is

$$G_{diff}(K_z,K_y,K_x=0)=\frac{\xi[1-\cos(K_z d)]}{w^2}\left[\frac{1-|\beta(K_y)|^2}{1-\cos(K_y a)}\right]. \quad (24)$$

Both Eqs. (22) and (24) have the right asymptotic behavior predicted for $K_y\to 0$. Thus the correlation length and the rms width of the steps determine the phase dependence of the diffuse shoulder over the total Brillouin zone.

IV. MONTE CARLO SIMULATION

Our MC simulations are based on a fcc lattice with a (111) surface instead of a (100) surface of the sc lattice used for the calculation of diffraction patterns. We choose these MC simulation conditions, since they are closer to realistic experimental conditions: there exist many studies on fcc samples, while only very few samples with sc structure are available.

As pointed out above, the diffraction pattern of the first Brillouin zone (which we analyze throughout this paper and which is also mostly investigated in other studies) is not influenced by the underlying lattice of the surface. This has also been demonstrated by MC simulations studying the growth on fcc(100) surfaces which additionally include shadowing effects of lower-level atoms at atomic steps.[29] Therefore the diffraction analysis developed for the sc lattice can be applied directly to the analysis of the MC data if one confines oneself to the first Brillouin zone.

If one applies the analytic results to the higher-order Brillouin zones of the fcc lattice, one has to consider an additional phase shift of $K_z=(2\pi/3d)(n-1)$ for the scattering condition for the nth Brillouin zone.

Since the details of the MC model used here are reported elsewhere,[30] we present only the basic features of the model. Generating the fcc lattice, we skewed an original sc lattice. The binding of the atoms on the sc lattice, however, mimics the binding configuration of an fcc lattice (e.g., a terrace atom has six bonds to adjacent terrace atoms and three additional bonds to atoms one layer underneath).

The hopping probability $\nu_{i,f}$ used for the MC simulations depends on both the local environment of the initial and the final coordination number (n_i and n_f, respectively) of the atom under interrogation via

$$\nu_{i,f}=\nu_0\exp\left[-\frac{E(n_i,n_f)}{kT}\right], \quad (25)$$

with activation energy

$$E(n_i,n_f)=n_i E_0+(n_i-n_f)E_b, \quad (26)$$

and effective attempt frequency $\nu_0=10^{13}$ s^{-1}. Here T denotes the sample temperature, and k the Boltzmann constant. Note that, for $E_b=0$, the final state does not influence the transition probability. Final-state effects can be caused by $E_b\neq 0$. It has been demonstrated that the diffusion is local isotropic for $E_b=0$, while $E_b\neq 0$ leads to locally anisotropic diffusion at steps.[30]

The simulations have been performed on lattices of 256×128 sites and eight equidistantly spaced terraces separated by one-atom-high steps, so that the initial terrace width is $L=16$ atoms. Screw-boundary conditions[16] are used in the

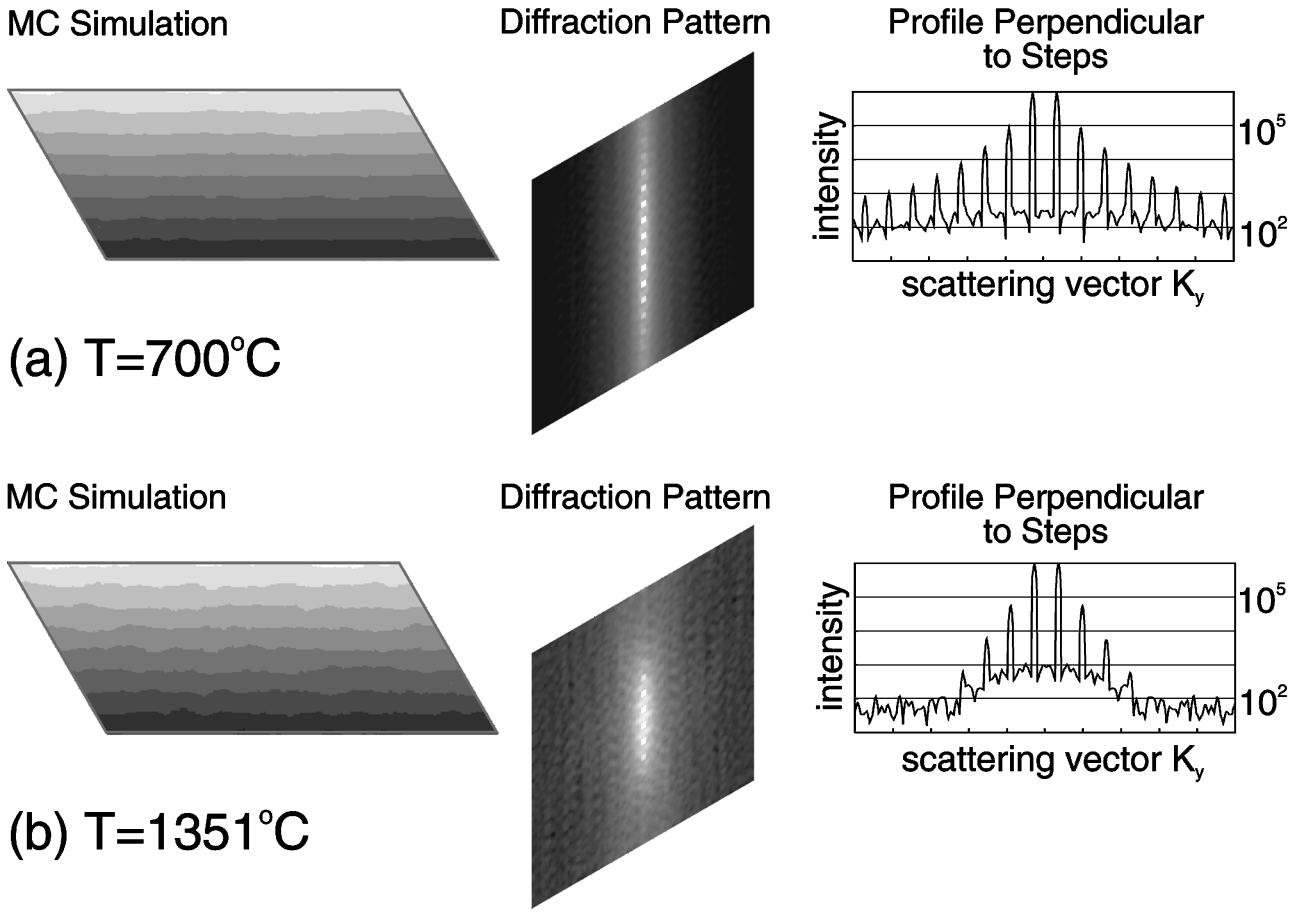

FIG. 5. Comparison of the MC simulated morphology, the 2D diffraction pattern at the vertical out-of-phase condition $K_z = \pi/d$, and cross sections of the diffraction pattern for $K_x = 0$ (from left to right) for (a) $T = 700\,^{\circ}\mathrm{C}$ and (b) $T = 1351\,^{\circ}\mathrm{C}$. With increasing temperature the step fluctuations and the diffuse background (streaked in the direction of the step train) increase, while the intensity of the sharp peaks decreases.

step train direction, while we used periodic boundary conditions parallel to the steps. All simulations start with uniform straight nonfluctuating steps. The MC simulations are performed until the kink density has reached a constant level (quasiequilibrium) for various temperatures. Since only next-neighbor bindings are used in the MC model, the probability to create vacancies and to nucleate islands increases with increasing temperature. This additional roughness of the terraces would complicate the diffraction analysis. Therefore the maximum temperature $T = 1351\,^{\circ}\mathrm{C}$ has been chosen to obtain rough meandering steps and almost flat terraces with negligible number of surface adatoms and monovacancies. For these configurations the diffraction patterns have been evaluated at the vertical out-of-phase condition $K_z d = \pi$ because of the maximum sensitivity of the diffuse scattering. The details of the time development have been reported elsewhere.[24]

We used $E_0 = 0.3$ eV and $E_b = 0.1$ eV for the study presented here. While the first parameter implies just the scaling of the temperature, the latter energy contribution causes an anisotropic diffusion. It enhances the diffusion along steps compared to the diffusion from steps onto the adjacent terrace, since the moving adatom has less nearest-neighbor atoms on a terrace site than on a step site. Therefore, the probability to detach adatoms from the step is suppressed by our ansatz of Eq. (26). This asymmetric diffusion has been reported from effective-medium theory calculations.[31] Furthermore, the formation of overhangs of the meandering step is also less probable for this case than for vanishing E_b.

V. RESULTS

Figure 5 shows the typical morphologies of the vicinal surfaces, the 2D diffraction patterns, and the line scans at $K_x = 0$ for the lowest and the highest studied temperatures (700 and 1351 °C, respectively) after having reached quasiequilibrium conditions. Obviously the roughness of the steps increases with increasing temperature. Nevertheless the average position of the steps is identical to the position when the simulation was started, so that the line scans for $K_x = 0$ show still sharp peaks at $K_y = [(2p+1)\pi/aL]$. In addition, the fluctuations are small compared to the width of the terraces, so that the meandering steps do not collide, suggesting that the fluctuations of adjacent steps are not correlated. In the following, we will analyze the diffraction pattern with respect to the spot profile evaluation presented above. In this paper, we would like to emphasize the analysis of the diffuse shoulder; we presented the attenuation effect of the sharp peaks previously.[24]

As predicted, the 2D diffraction patterns show a streaked diffuse intensity in the direction of the step train in addition to residual sharp peaks caused by the perfect regularly ar-

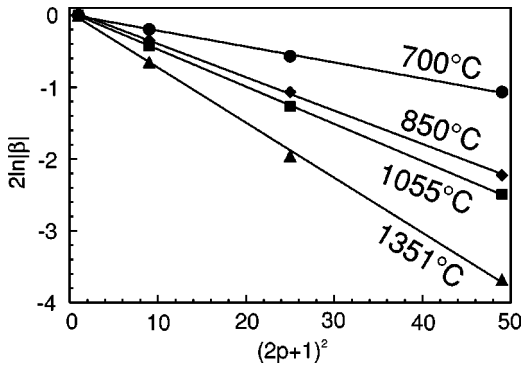

FIG. 6. Attenuation of the intensity of the sharp peaks for different temperatures. With increasing temperature, the attenuation is stronger. The straight lines demonstrate that Eq. (9) is fulfilled, so that one can evaluate the rms width w of the steps from the slope.

ranged *average* step position. The intensity of the sharp pattern decreases drastically (especially for the higher-order peaks) with increasing temperature while the diffuse intensity increases. All eight orders of peaks expected for the regularly stepped surface can be seen for 700 °C, but only four orders can be distinguished from the diffuse background for 1351 °C.

Both the 2D diffraction patterns and the line scans presented in Fig. 5 demonstrate that the structure of the diffuse scattering does not depend strongly on K_y for small fluctuations ($T=700$ °C). The diffuse scattering shows an increasing intensity at the center of the Brillouin zone for increasing step roughness, as predicted by Eq. (24).

Following Eq. (5) the intensity of the sharp pth order peak (position $K_y=[(2p+1)\pi/aL]$) is attenuated by

$$|\beta|^2=\exp\left[-\frac{w^2}{a^2}\left(\frac{(2p+1)\pi}{L}\right)^2\right] \tag{27}$$

for the lower-order peaks. Figure 6 demonstrates that the attenuation depends on the square of the diffraction order for all temperatures and for $p\leqslant 4$. Fitting the MC simulated results to Eq. (27), we are able to evaluate the rms width w from the diffraction pattern. Figure 7 shows the excellent one-to-one agreement between the rms width w_{MCS} obtained by analyzing directly the step roughness from the MC simulation (cf. Fig. 5), and w_{diff} from the diffraction analysis (cf. Fig. 6). Additionally, the inset shows the increasing rms width of the steps with increasing temperature. For more details, see Ref. 24, where the physical processes of the thermal roughening are discussed more explicitly; in this study we concentrate on the diffraction analysis.

Figure 8 shows the diffraction pattern integrated parallel to the steps (open dots). The scaling has been chosen to emphasize the diffuse scattering. Therefore not all sharp peaks can be seen. Obviously the slit-integrated diffuse profile becomes more peaked with increasing step roughness. The solid line shows the diffuse shoulder predicted by Eq. (14). The only parameter fitted to the profiles is the peak intensity at $K_y=0$. For the evaluation of the profiles we have used the rms width obtained from the analysis of the peak intensity attenuation (cf. Fig. 7), which gives the correct value for the noncorrelated step fluctuations.

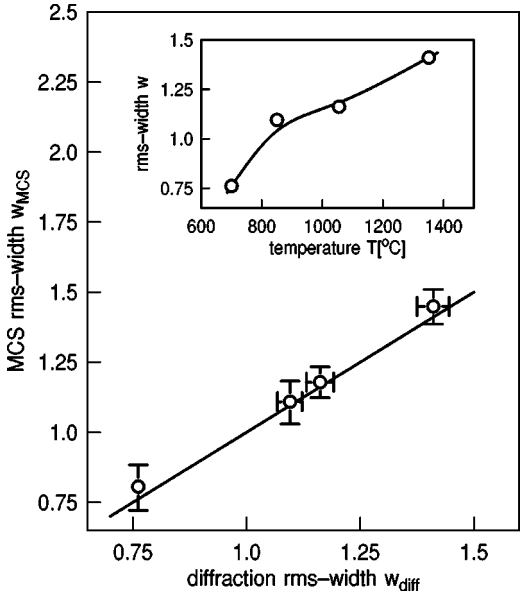

FIG. 7. Comparison of the rms width of the meandering obtained directly from analyzing the MC simulation pictures w_{MCS} and from analyzing the attenuation of the intensity of the sharp peaks w_{diff}. The solid line shows the perfect one-to-one agreement. The inset shows the temperature dependence of the rms width. With increasing temperature, the step fluctuations increase.

For $K_x=0$, Fig. 9(a) shows the line scan for the largest step roughness investigated here ($T=1351$ °C). Only four orders of sharp peaks can be distinguished from the background. Figure 9(b) presents line scans of the diffuse shoulder parallel to the steps (open symbols) for a fixed K_y, as labeled in Fig. 9(a). Fitting the data to Lorentzians yields the solid lines shown. The line scans also demonstrate that the

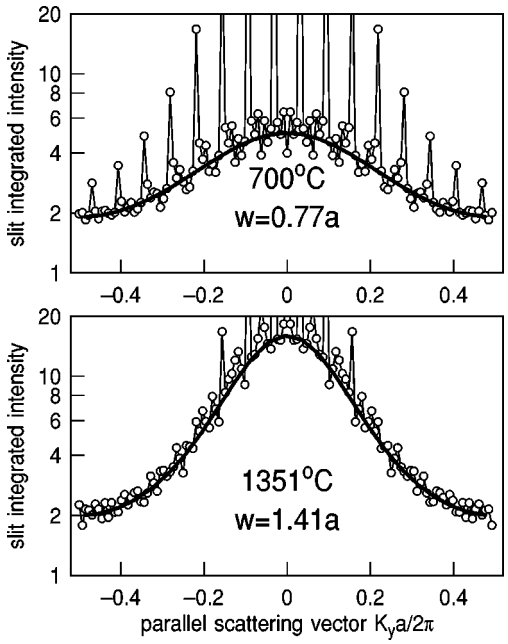

FIG. 8. Profiles from slit integrating the diffuse intensity parallel to the steps (open dots). The solid lines show the diffuse scattering following Eq. (14). The rms width w entering the evaluation has not been fitted, but is taken from Fig. 7. The agreement between theory and MC simulations is perfect.

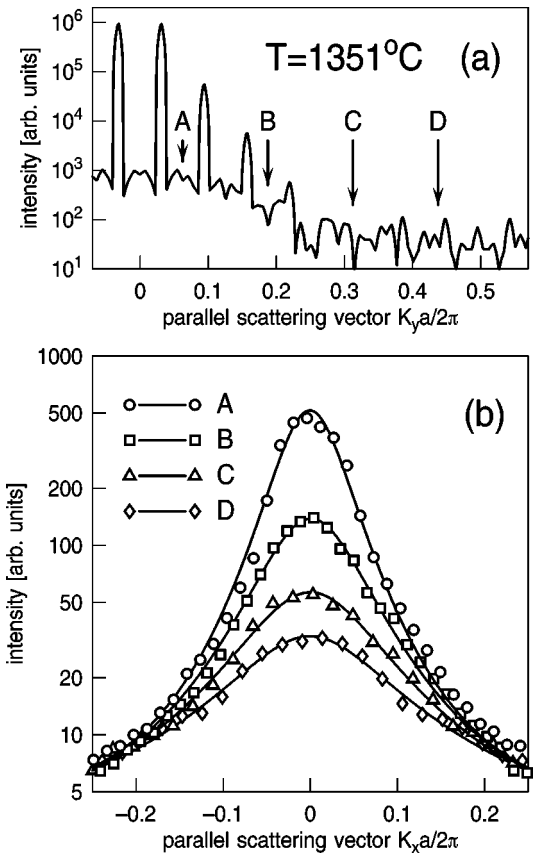

FIG. 9. Diffraction pattern for $T=1351\,^{\circ}\mathrm{C}$. (a) Line scan for $K_y=0$ showing the diffuse scattering and the sharp peaks due to the long-range order of the steps. (b) Profiles of the diffuse scattering taken at the scattering conditions labeled in (a). With decreasing scattering vector K_y, the profiles become sharper and more intense. The line scans *A*, *B*, *C*, and *D* are equidistant, taken exactly at positions between two sharp peaks to emphasize the diffuse profiles parallel to the steps.

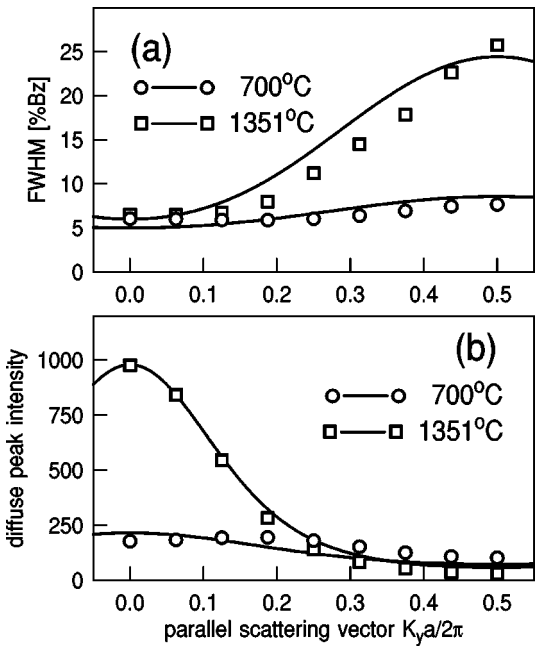

FIG. 10. Analysis of the diffuse scattering depending on the perpendicular scattering vector K_y from fitting profiles with Lorentzian shape for $T=700$ and $T=1351\,^{\circ}\mathrm{C}$. (a) *Half-width*. While the half-width is almost constant for $T=700\,^{\circ}\mathrm{C}$, it increases with increasing scattering vector for $T=1351\,^{\circ}\mathrm{C}$. (b) *Peak intensity of the diffuse scattering*. The diffuse scattering becomes more pronounced with increasing step roughness ($T=1351\,^{\circ}\mathrm{C}$). The solid lines for both figures follow Eqs. (22) and (24), taking the rms width from Fig. 7.

peak intensity of the diffuse shoulder decreases with an increasing distance from the center of the Brillouin zone, and that the half-width of the shoulder increases.

A more detailed analysis of the diffuse shoulder profiles recorded for scattering conditions $K_y=2\pi p/aL$, half between the positions of the sharp peaks, is shown in Fig. 10. For comparison, the analysis for $T=700\,^{\circ}\mathrm{C}$ is included. Obviously, the behavior of both surfaces is very different. For $T=700\,^{\circ}\mathrm{C}$, both the maximum intensity and the half-width of the diffuse shoulder are almost constant. This is in good agreement with our analysis for small fluctuations (two-level model), although the evaluated rms width of $w=0.75a$ is slightly larger than the maximum value for the two-level model ($w=0.5a$) with equally distributed step chords on both levels.

There are drastic variations of both the peak intensity and the half-width for $T=1351\,^{\circ}\mathrm{C}$. Compared to $T=700\,^{\circ}\mathrm{C}$ the maximum intensity is high, while the half-width does not change drastically for the lateral in-phase condition $K_y=0$. This implies that the correlation length ξ does not vary strongly with temperature. The half-width, however, increases with increasing temperature for the lateral out-of-phase condition $K_y=\pi/a$, indicating that the kink density increases with temperature.

The solid lines shown in Fig. 10 correspond to the predicted behavior [according to Eqs. (22) and (24)]. Again the shape of the lines has not been fitted. Since the rms width w was obtained from analyzing the intensity of the sharp peaks (cf. Fig. 7) the only parameters adjusted are the FWHM at the out-of-phase condition and the maximum intensity at the in-phase condition for (a) and (b), respectively. The agreement for the intensity is perfect and reasonable for the half-width.

Comparing the kink density ρ obtained directly from the MC simulation with the kink density evaluated from the half-width of the diffuse shoulder shows excellent agreement. Figure 11 demonstrates that the predicted behavior is fulfilled for all studied surfaces: a FWHM equal to 4ρ (solid line, no fitting parameter). We conclude from the Lorentzian shape of the diffuse scattering that the kink-kink distance distribution is geometric. This implies that the kinks are distributed randomly at the meandering steps so that the kink-kink interaction is very weak.

Increasing the temperature increases the kink density. The inset of Fig. 11 shows additionally that the kink density follows an Arrhenius behavior for our MC simulations. We obtain the energy of $E_{\mathrm{kink}}=0.26$ eV for the formation of kinks, which is in excellent agreement with the expected value of $E_{\mathrm{kink}}=\frac{1}{2}E_0+E_b$.[24]

VI. DISCUSSION AND CONCLUSION

In this paper we have presented a diffraction analysis of the diffuse scattering for vicinal surfaces with noncolliding

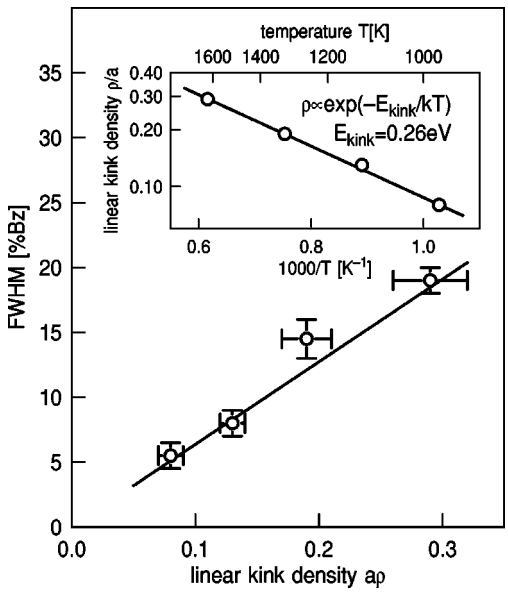

FIG. 11. Comparison of the kink density ρ obtained from directly analyzing the MC simulation pictures and from analyzing the diffuse scattering at the out-of-phase scattering at the boundary of the Brillouin zone. The solid line shows that the predicted FWHM is equal to 4ρ. The inset shows an Arrhenius plot of the kink density from which one obtains the kink formation energy $E=0.26$ eV.

meandering steps. The analysis was performed for various rough surfaces generated by MC simulations at the vertical out-of-phase condition required for terraces ($K_z=[(2n+1)\pi/d]$) to have maximum sensitivity to the surface roughness. In the following, first, we will discuss the results of the diffuse scattering profile analysis. Since the key point is that adjacent steps do not collide, and that fluctuations of neighbor steps are not correlated we will demonstrate that the MC simulations performed here are well suited to fulfilling this conditions. Finally, we show that this analysis can also be applied to diffuse x-ray-diffraction analysis from multilayers.

Our study shows that different roughness parameters such as the rms width w, the correlation length ξ, and the kink density ρ of the meandering steps can be obtained by analyzing profiles of the diffuse shoulder for different lateral scattering conditions. The rms width w characterizing the perpendicular step fluctuations can be evaluated from the diffuse profile in the direction of the step train (perpendicular to the steps) for $K_x=0$. One has to use line scans parallel to the steps at different lateral scattering conditions to obtain the two roughness parameters ξ and ρ characterizing the roughness parallel to the steps. While the correlation length ξ governs the diffuse profile for the lateral in-phase condition $K_y=0$ (the line scan including the center of the Brillouin zone) the kink density ρ determines the profile at the lateral out-of-phase condition $K_y=\pm\pi/a$ (the line scan at the boundary of the Brillouin zone).

Also striking is the effect of the residual sharp peaks even at the roughest surfaces studied here, which are only attenuated by the increasing step fluctuations. This is a clear effect of the noncolliding steps, preserving the long-range order of the steps. It has been shown previously by many authors for 1D surfaces that the loss of long-range order yields the broadening of the peaks, presuming that the sizes of adjacent terraces are not correlated.[1,4–6]

This effect can also be included in the analysis presented here if one drops the constraint of average equidistant steps. Assuming also that the *average* step-step distance fluctuates (averaging with respect to the coordinate x along the step) Eq. (7) can be modified to include these effects. This leads to a broadening of the sharp peaks perpendicular to the steps governed by the distribution of average terrace sizes. Here we define the average terrace size by the distance between two neighbor steps where the position of the step is obtained from the average step position eliminating the fluctuations.

Furthermore, we would like to stress the point that the noncolliding of the steps is not the only assumption of our analysis. Previously, we investigated the diffraction pattern from vicinal surfaces with strongly correlated steps [$u_n(x)=u(x)$ for *all* steps].[6] This substantially affects the evaluation of the diffraction pattern. The main result is that the diffuse shoulder is constricted to lateral scattering vectors close to the center of the Brillouin-zone. Hence one cannot perform the kink density analysis from the spot profiles at the Brillouin zone boundary. Nevertheless, the analysis of diffraction spot profiles close to the center of the Brillouin zone yielding the correlation length and the rms width is still possible.

We obtained Lorentzian profiles at the lateral out-of-phase scattering condition. Therefore the kink-kink distance distribution is geometric, and the kinks are distributed statistically at the single steps. If there is a kink-kink repulsion, one would obtain a preferential kink-kink distance and a peaked kink-kink distance distribution. For these conditions the profiles would split into satellites at $K_y=\pm\pi/a$ and $K_x=\pm\pi/\langle D\rangle$, where $\langle D\rangle$ denotes the average kink-kink distance. For different lateral scattering conditions K_y, the position of the satellite may shift closer to $K_x=0$. This situation is similar to the diffraction pattern obtained for 1D surfaces with preferential terrace size, where one observes a maximum splitting of the satellites at the (vertical) out-of-phase condition, while the satellites move closer to the specular beam for scattering conditions closer to the (vertical) in-phase condition.[5]

The standard analysis for the surface roughening transition predicts logarithmic correlation functions for the rough phase, yielding power laws for the spot profiles.[11,15,16,32,33] The authors of Ref. 14, however, showed that the shape of profiles parallel to the steps taken at $K_y=\pi/aL$ (the position of the first-order peak) have different scaling behaviors depending on the considered range of K_x. The logarithmic behavior can only be observed for $K_x<1/x_{coll}$, while a Lorentzian shape governs the profiles at $1/x_{coll}<K_x<2\pi/a$, where x_{coll} denotes the lateral distance between step collisions. Therefore we can explain the Lorentzian profiles by the fact that we do not observe any step collisions for the temperatures studied here (cf. Fig. 5), so that we propose $x_{coll}>aL$.

Reference 14 also presented the estimate $x_{coll}\simeq L^2a^3/4b^2$ of the average collision distance (we would like to remark that the factor a^3 appears here because L denotes the average *number* of terrace atoms between two adjacent steps, while Ref. 14 denoted the average *distance* by L). From our kink density analysis of the diffusivity, we can also calculate the average collision distance $x_{coll}\simeq L^2/4\rho$ ranging from 800 to 220 lattice sites for the investigated temperature

range 700–1351 °C. This underpins the impression of negligible step collisions even at the highest temperatures, because we performed the MC simulation on a lattice with size $L_x=256$ parallel to the steps (cf. Fig. 5). Since we do not observe any step collisions in our MC simulations even at the highest temperatures reported here [cf. Fig. 5(b)], it seems that the above expression for x_{coll} underestimates the collision distance.

This effect is also important for the interpretation of experiments. The lattice size for the MC simulation is equivalent to the instrumental resolution of a diffraction apparatus. Therefore, one may have the impression of a well-ordered vicinal surface with slightly fluctuating steps if the average step collision distance is larger than the transfer width of the instrument.

We mention that we also studied the surface roughness at higher temperatures, where we observed both effects of step collisions and of additional roughening of the terraces. This, however, will be subject of a forthcoming report.

The spot profile analysis of Ref. 14 concentrated on profiles parallel to the steps at $K_y=\pi/aL$ to study the transition from power-law to Lorentzian profiles depending on the distance of step collisions. The authors showed that the half-width of the Lorentzian is governed by the correlation length ξ. On the other hand, here, we study in detail the diffraction from vicinal surfaces in the temperature range where step collisions are negligible. We obtain roughness parameters from line scans parallel to steps at different scattering conditions. The correlation length ξ also governs the line scans at the center of the Brillouin zone. Because this scattering condition is close to $K_y=\pi/aL$ (usually L is sufficiently large) the only difference between both studies is the prefactor between half-width and inverse correlation length which can be explained by Eq. (22).

Furthermore, we have demonstrated that one obtains the kink density (to be more accurate, the kink distance distribution) from the line scans at the Brillouin-zone boundary. Connecting the correlation length and kink density, we are able to determine the diffusivity $b^2(T)$ proportional to the kink density (cf. also Ref. 27). Therefore, the temperature dependence of both is identical following an Arrhenius behavior corresponding to the kink energy $E_{\mathrm{kink}}=0.26$ eV.

Finally, we emphasize that the diffraction spot evaluation presented here can also be applied to x-ray studies from multilayers using the out-of-phase condition perpendicular to terraces, and considering the scattering vectors K_x and K_y as parallel and perpendicular to the interfaces of the multilayer, respectively. In this picture adjacent terraces can be considered as adjacent layers. Using the scattering condition $K_z=\pi/d$ for the vicinal surface leads to a maximum contrast between adjacent terraces associated with scattering amplitudes ± 1. Usually, the contrast between adjacent layers is due to different (complex) scattering amplitudes (including scattering phase differences). This, however, affects only the total intensity of the diffuse scattering and of the sharp peaks.

Since, in contrast to the infinite number of terraces for vicinal surfaces, multilayers have only a finite number of layers the sharp peaks are not δ function like sharp but show a finite width corresponding to the total thickness of the multilayer. Additionally, for very thick multilayers the reduced reflected intensity due to absorption of the beam has to be taken into account. In this sense Fig. 9(a) corresponds to the $(\theta,2\theta)$ specular scans normal to the multilayer, and Fig. 9(b) to transverse scans (rocking curves) parallel to it.

From x-ray measurements from W/C multilayers, it has been reported that the diffuse scattering is focused in scattering planes parallel to the multilayer at the 3D Bragg condition.[25] This effect has been explained by the partial correlation of interfacial fluctuations.[34,35] The 3D Bragg condition is equivalent to $K_y=0$ in our study. Figure 9 clearly shows that this focusing effect can also be produced by interfaces with noncorrelated fluctuations if the rms width is not too small and if the off-specular scanning condition $(K_x\neq 0)$ is not too large. The focusing effect due to partial interface correlations is much larger than the one we observe here for noncorrelated rough interfaces.

In summary, we have shown that the analysis of the diffuse scattering from vicinal surfaces with noncolliding steps is a powerful method to obtain statistical information about the roughness of the steps as well as the kink density, the correlation length, and the rms width of the meandering steps. For this purpose, we have analyzed line scans for the diffuse scattering in different directions and for different lateral scattering conditions. While line scans at the Brillouin-zone boundary are only sensitive to the kink distance distribution, line scans at the center of the Brillouin zone are governed by the correlation length. Since for rough surfaces the correlation length is much larger than the average kink distance the diffuse scattering at the Brillouin-zone boundary is broader than at the center of the Brillouin zone. Furthermore, long-range order with negligible step collisions conserves the ideal positions of the sharp peaks. In addition, step collisions broaden these spots, so that one is able to distinguish both kinds of step roughness easily.

ACKNOWLEDGMENTS

Helpful discussions with M. C. Tringides are gratefully acknowledged. This work was supported by the Alexander von Humboldt Foundation and the Swedish Research Council for Engineering Sciences.

*Permanent address: University of Karlstad, Department of Engineering Science, Physics and Mathematics, S-65188 Karlstad, Sweden. Electronic address: mats.larsson@hks.se

[1] P. R. Pukite, C. S. Lent, and P. I. Cohen, Surf. Sci. **167**, 39 (1985).
[2] J. M. Pimbley and T. M. Lu, J. Appl. Phys. **55**, 182 (1984).
[3] M. Henzler, Surf. Sci. **152/153**, 963 (1985).
[4] M. Presicci and T. M. Lu, Surf. Sci. **141**, 233 (1984).
[5] J. M. Pimbley and T. M. Lu, Surf. Sci. **159**, 169 (1985).
[6] J. Wollschläger, Surf. Sci. **383**, 103 (1997).
[7] M. C. Bartelt and J. W. Evans, Phys. Rev. Lett. **75**, 4250 (1995).
[8] J. A. Stroscio, D. T. Pierce, M. D. Stiles, A. Zangwill, and L. M. Sander, Phys. Rev. Lett. **75**, 4246 (1995).
[9] J. G. Amar and F. Family, Surf. Sci. **365**, 177 (1996).

[10] J. W. Evans and M. C. Bartelt, Langmuir **12**, 217 (1996).
[11] J. Villain, D. R. Grempel, and J. Lapujoulade, J. Phys. F **15**, 809 (1985).
[12] R. Kariotis, B. S. Swartzentruber, and M. G. Lagally, J. Appl. Phys. **67**, 2848 (1989).
[13] J. Kleiner, C. E. Aumann, Y. W. Mo, R. Kariotis, and M. G. Lagally, Surf. Sci. **240**, 293 (1990).
[14] N. C. Bartelt, T. L. Einstein, and E. D. Williams, Surf. Sci. **276**, 308 (1992).
[15] W. Selke and A. M. Szpilka, Z. Phys. B **62**, 381 (1986).
[16] N. C. Bartelt, T. L. Einstein, and E. D. Williams, Surf. Sci. **244**, 149 (1991).
[17] T. L. Einstein, N. C. Bartelt, J. L. Goldberg, X. S. Wang, E. D. Williams, and B. Joos, in *The Structure of Surfaces III*, edited by S. Y. Tong, M. A. Van Hove, K. Takayanagi, and X. D. Xie, Springer Series in Surface Science Vol. 24 (Springer, Berlin 1991), p. 486.
[18] M. den Nijs, E. K. Riedel, E. H. Conrad, and T. Engel, Phys. Rev. Lett. **55**, 1689 (1985).
[19] J. Lapujoulade, Surf. Sci. **178**, 406 (1986).
[20] E. H. Conrad, L. R. Allen, D. L. Blanchard, and T. Engel, Surf. Sci. **187**, 265 (1987).
[21] B. Salanon, F. Fabre, J. Lapujoulade, and W. Selke, Phys. Rev. B **38**, 7385 (1988).
[22] H. N. Yang, T. M. Lu, and G. C. Wang, Phys. Rev. Lett. **63**, 1621 (1990).
[23] J. Wollschläger, E. Z. Luo, and M. Henzler, Phys. Rev. B **44**, 13 031 (1991).
[24] M. I. Larsson, M. Tringides, H. Frischat, and J. Wollschläger, Surf. Sci. **387**, 142 (1997).
[25] D. E. Savage, J. Kleiner, N. Schimke, Y. H. Phang, J. Jacobs, R. Kariotis, and M. G. Lagally, J. Appl. Phys. **69**, 1411 (1991).
[26] M. Henzler, in *Reflection High-Energy Electron Diffraction and Reflection Electron Imaging of Surfaces*, edited by P. K. Larsen and P. J. Dobson (Plenum, New York, 1988), p. 193.
[27] N. C. Bartelt, T. L. Einstein, and E. D. Williams, Surf. Sci. **240**, L591 (1990).
[28] J. Wollschläger, E. Z. Luo, and M. Henzler, Phys. Rev. B (to be published).
[29] H. C. Kang, D. K. Flynn-Sanders, P. A. Thiel, and J. W. Evans, Surf. Sci. **256**, 205 (1991).
[30] M. I. Larsson, H. Frischat, J. Wollschläger, and M. Tringides, Surf. Sci. **381**, 123 (1997).
[31] J. Jacobsen, K. W. Jacobsen, P. Stoltze, and J. K. Norskøv, Phys. Rev. Lett. **74**, 2295 (1995).
[32] H. van Beijeren and I. Nolden, in *Structure and Dynamics of Surfaces II*, edited by W. Schlommers and P. von Blankenhagen, Topics in Current Physics Vol. 43 (Springer, Berlin, 1987), p. 259.
[33] T. Engel, in *Chemistry and Physics of Solid Surfaces VII*, edited by R. Vanselow and R. Howe, Springer Series in Surface Science Vol. 10 (Springer, Berlin, 1988), p. 407.
[34] Y. H. Phang, R. Kariotis, D. E. Savage, and M. G. Lagally, J. Appl. Phys. **72**, 4627 (1992).
[35] Y. H. Phang, D. E. Savage, R. Kariotis, and M. G. Lagally, J. Appl. Phys. **74**, 3181 (1993).